Insights into the mechanism of electrocatalytic CO2 reduction and concomitant catalyst degradation pathways

Raaijman, S.J.

4

Clean and Reproducible Voltammetry of Copper Single Crystals with Prominent Facet-Specific Features Using Induction Annealing

Although copper is widely used as an electrocatalyst for the CO_2 reduction reaction, often little emphasis is placed on identifying exactly the facet distribution of the copper surface. Furthermore, because of differing surface preparation methodologies, reported characterization voltammograms (where applicable) often vary significantly between laboratories, even for surfaces of supposedly the same orientation. In this work, we describe a surface preparation methodology involving the combination of induction annealing and well-documented electrochemical steps, by which reproducible voltammetry for copper surfaces of different orientations can be obtained. Specifically, we investigated copper surfaces of the three principal orientations: (111), (100) and (110), and a representative polycrystalline surface. We compared these surfaces to surfaces reported in the literature prepared via either electropolishing or UHV-standard methodologies, where we find induction preparation to yield improvements in surface quality with respect to electropolished surfaces, though not quite as good as those obtained by UHV-preparation.

This chapter has been published in
Raaijman, S. J.; Arulmozhi, N.; da Silva, A.H.M.; Koper, M. T. M., *J. Electrochem. Soc.* **2021**, *168* (9) 096510

4.1. Introduction

With a paradigm shift in climate-related research, copper has found itself at the frontier of investigations into electrochemical carbon dioxide reduction (i.e., the CO_2 reduction reaction, CO2RR) due to its unique propensity to generate $> 2\,e^-$ and C2+ products from CO_2. The product spectrum is found to be strongly influenced by both potential[1–3] and the specific facet distribution at the interface[4, 5] with e.g., ethylene formation having higher yields at lower overpotentials on the {100} plane compared to the {111} and {110} faces.[4, 6, 7] This shows the importance of identifying and reporting the types of electrochemically active sites present on copper surfaces used to study the CO2RR. Means of characterizing differing copper sites have been described previously in the works of e.g., Jović and Jović[8, 9], Schouten *et al.*[10], and more recently in more detail by Engstfelt *et al.*[11], Bagger *et al.*,[12] Maagaard *et al.*[13], Sebastián-Pascual *et al.*[14, 15], and Tiwari *et al.*[16–18] However, metallic copper proves to be very exacting in terms of its treatment, both prior to and during electrochemical characterization – often leading to surfaces prepared under similar conditions exhibiting substantial differences in their electrochemical fingerprint.[11, 18]

Surface preparation, specifically, plays an important role in obtaining reproducible surfaces. Considering copper's propensity to oxidize, it is not possible to employ the current default preparation methodology for (more) noble metals: i.e., flame annealing under ambient conditions, as first introduced by Clavilier *et al.*[19] As such, different preparatory treatments were established for copper surfaces. These methodologies are electrochemical in nature: several copper layers are removed by forming, and subsequently dissolving, copper oxides[20] through subjecting the surface to oxidizing potentials in concentrated phosphoric acid solution (generally with respect to a copper or graphite counter electrode in a two-electrode configuration).[2, 10] However, this so-called electropolishing is anisotropic, and thus the resulting facet distribution will be a function of applied potential and polarization time. Since potentials are commonly applied in a two-electrode configuration, the exact potential at the electrode interface is ill-defined, leading to further discrepancies between different samples and surfaces prepared in different laboratories.

Therefore, although we have means of preparing and characterizing (single-crystalline) copper surfaces, we currently lack exact methodologies to systematically and consistently generate reproducible surfaces that yield identical results among different laboratories. In this work, we extend the commonly employed methodologies for the preparation of copper surfaces with induction annealing to obtain improved surface reproducibility with relatively little impact on experimental complexity. We will describe a set of experimental steps consisting of a combination of electropolishing, electromagnetic induction heating, and specific electrochemical treatments that yield reproducible copper surfaces with clear facet-specific adsorption features for commonly studied copper surfaces; Cu(111), Cu(100), Cu(110) and Cu(poly). We will compare our results to results obtained by electropolishing only, and to surfaces prepared in ultra-high vacuum (UHV), which would be the preferred methodology but is more cumbersome and also not widely available.

4.2. Experimental

4.2.1. Chemicals, electrochemistry and cells

All solutions were made by dissolving appropriate amounts of chemicals in Milli-Q water (Millipore, resistivity $\geq 18.2\ M\Omega \cdot cm$). The chemicals: H_3PO_4 (85%, p.a., Merck), H_2SO_4 (96%, ACS reagent, Honeywell), H_2O_2 (35%, Ph. Nord, Merck), HNO_3 (65%, Ph. Eur., Boom), $KMnO_4$ (ACS reagent, Sigma Aldrich), NaOH (99.99%, trace metals basis, Sigma Aldrich) for preparing electrolyte, and NaOH (30.4%, Suprapur, Supelco) for the $10\ M$ oxidation experiment in Figure 4.8, were used without further purification. Gases, H_2 (Linde 5.0) and Ar (Linde, 5.0), were used as received.

The experimental work was conducted using monocrystalline disk-type Cu(111), Cu(100) and Cu(110) electrodes (Surface Preparatory Labs, oriented to $\leq 0.1°, d = 8\ mm$), and spherical bead-type and disk-type polycrystalline Cu(poly) working electrodes (WEs). Cu(poly) disk-type electrodes were made by machining a Cu foil (99.995%, Mateck) into the desired shape and dimension (disk of $d = 10\ mm$) and laser welding a copper wire to the backside. Cu(poly) spherical bead-type electrodes of ca. $2-3\ mm$ in diameter were made by melting a copper wire (99.9999%, metals basis, Puratronic) into a droplet via induction annealing under oxygen-free atmosphere (H_2 or Ar). Surface impurities were removed by briefly etching (ca. $5\ s$) the resulting bead electrode in concentrated nitric acid (65%), and re-melting the bead (but not allowing it to grow larger). This etching/remelting cycle was repeated ca. 4 times to remove the majority of visible surface contaminants.

WEs were cleaned either by mechanical polishing followed by sonication and electropolishing (for the machined Cu(poly) disk-type electrode) or via induction annealing (all other electrodes) prior to each measurement, with the exact methodologies described in more detail in the supporting information (SI). Characterization CVs ($0.1\ M$ NaOH) were obtained following facet-specific procedures involving insertion at particular potentials and pre-cycling in specific potential windows prior to measuring the 'full-scale' CVs given in this work. Exact parameters are detailed in the SI. A reversible hydrogen electrode (RHE) (Hydroflex, Gaskatel) was used as a reference electrode (RE). All potentials in this work are reported vs. RHE unless specified otherwise. A platinum spiral ($99.99 + \%$) was used as a counter electrode (CE), and was cleaned in concentrated piranha solution ($3:1\ v/v$ mix of H_2SO_4 and H_2O_2) overnight after disassembly of the cell to remove any copper contaminants. After piranha exposure, Pt CEs were flame annealed prior to insertion into the cell.

Glassware and plasticware were cleaned in acidified aqueous permanganate solution for $12+\ hours$ ($0.5\ M\ H_2SO_4 + 1\ g \cdot L^{-1}\ KMnO_4$). Prior to starting experiments, the leftover cleaning solution was removed by rinsing with Milli-Q water and washing with diluted piranha solution (diluted to $> 95\ vol\%$ water) to remove manganese dioxide and permanganate residue. Next, glassware/plasticware was rinsed three times and boiled five times in Milli-Q water to remove piranha residue.

A one-compartment fluorinated ethylene propylene (FEP) cell, fitted with ETFE gas tubes and holes for the RE and CE, was used for electrochemical measurements. Electrolyte solutions were prepared by dissolving appropriate amounts of chemicals in Milli-Q water. Argon was passed through and above the electrolyte to remove

any dissolved gases. Prior to closing the electrical circuit, argon flow through the electrolyte was stopped while argon flow above the electrolyte was initiated or maintained. Disk electrodes were measured in hanging meniscus configuration, whereas spherical bead-type electrodes were inserted with the entirety of the bead submerged, with the electrolyte level reaching to where the bead was connected to the wire. Where applicable, CVs were normalized to the geometric surface area, except in the case of spherical bead-type Cu(poly) electrodes, which were normalized to their OH-adsorption charge as measured between $-0.25\ V < E < +0.44\ V$ after correcting for the double layer current. The value used for conversion of OH-adsorption charge to area was $128.1\ \mu C \cdot cm^{-2}$, which was determined as described in the SI.

4.2.2. Instruments and Software

A BioLogic VSP-300 potentiostat controlled via their proprietary software EC-Lab was used for all electrochemical measurements. Literature CVs were extracted from their respective sources in image form and converted to numeric data using the shareware 'DataThief III'. Data editing and plotting was done using the software Igor. Mass flow controllers (SLA5850, Brooks) were digitally controlled via the manufacturer's proprietary software. Where applicable, mechanical polishing was conducted on a Forcipol 1 machine (Metkon), post-polishing ultrasonication was done in a Bandelin Sonorex RK 25 H ultrasonicator and RF heating was applied via a 2.4 kW Ambrell EASYheat model 0224 fitted with a Flowmax water cooling solution.

4.2.3. Normalization of literature CVs

Digitized literature CVs were edited in a number of ways to facilitate comparison to our CVs. Firstly, they were manually shifted horizontally to achieve symmetry of the main adsorption feature around the x-axis (to offset ORR-related current). Secondly, where applicable, the potential was shifted to best align key adsorption features (any such shifts are specified in the legend). Thirdly, they were scaled such that they yielded identical double layer (DL) thicknesses (defined as $i^{average}_{forward\ scan} - i^{average}_{backward\ scan}$) within a potential region where all CVs of the same surface orientation exhibited (apparent) capacitive behavior. Specifically, these regions were $+0.225\ V < E < +0.275\ V$, $+0.17\ V < E < +0.24\ V$ and $-0.10\ V < E < +0.10\ V$ for Cu(111), Cu(100) and Cu(110) surfaces, respectively. The potential boundaries were chosen as large as possible to average out any inaccuracies from the image to data transcription process. Although we will refer to these areas as double layer regions, an important secondary consideration in picking these particular boundaries was the degree of overlap between CVs of different sources. As such, these regions are not necessarily representative of what we would consider ideal locations for determining the double layer capacity for these surfaces.

4.3. Results and discussion

4.3.1. Literature comparison

To verify the quality of the surfaces obtained via our methodology, CVs of the three basal planes ({111}, {100} and {110}) are compared to recent literature discussing UHV-prepared crystals and electropolished surfaces from sources that report CVs with clear facet-specific features (Figures 4.1-4.3). The CVs we report were measured in $0.1\ M$ NaOH, whereas it is common in recent literature to use $0.1\ M$ KOH. Cations of different identity may have an effect on peak intensity: Engstfeld *et al.* show peak suppression for the Cu(100)-specific feature in KOH compared to NaOH electrolyte[11], although Tiwari *et al.* show only minor differences exists for Cu(111) when comparing KOH and NaOH electrolytes.[18] DFT calculations predict that the presence of a cation should have little effect on adsorption energies on copper surfaces (and thus the CV)[21], but no systematic experimental study exists (to the best of our knowledge). Other experimental conditions, such as molarity ($0.1\ M$) and scan rate ($\nu = 50\ mV \cdot s^{-1}$) are the same for all discussed CVs, as is the cell material (plastic) for all but one of the CVs (electropolished Cu(110) by Huang *et al.*[22], which was likely measured in glass judging by their reported Cu(111) CV, though not specified in text).

Cu(111) literature comparison

In Figure 4.1, CVs of Cu(111) as obtained via various preparation methods are depicted. Black represents a UHV-prepared surface[17], with an electropolished sample by the same group shown in orange.[17] Another electropolished crystal, from a different group, is shown in red[15], and the CV obtained by us is in blue. As can be seen, all CVs exhibit a strong reversible adsorption feature centered around $+0.1\ V$[18], which has been assigned to OH-adsorption on {111} terraces.[17, 23] An additional {111}-related peak is seen for the blue CV at $+0.455\ V$ (presumably O-adsorption, further elaborated in a later section). However, scanning to such oxidative potentials results in irreversible surface changes thus necessitating reannealing of the crystal to regain surface ordering.

Comparing the black (UHV) and orange (electropolished) CVs we find that an electropolished surface measured by the same group exhibits suppressed intensity for the OH-adsorption feature; a common characteristic for electropolished samples. However, fair comparison between differing sources is impeded by a specific characteristic of the {111} facet: namely that it apparently requires active cycling. Specifically, by only briefly applying a standby potential before initiating cycling, such as done by Sebastián-Pascual *et al.* for their electropolished CV (red)[15], the DL-normalized {111}-specific feature at $+0.1\ V$ becomes more pronounced compared to Tiwari *et al.*'s UHV-prepared surface.[17] Considering we employ the same electrochemical methodology, also our CV (blue) exhibits a similarly more intense OH-adsorption feature.

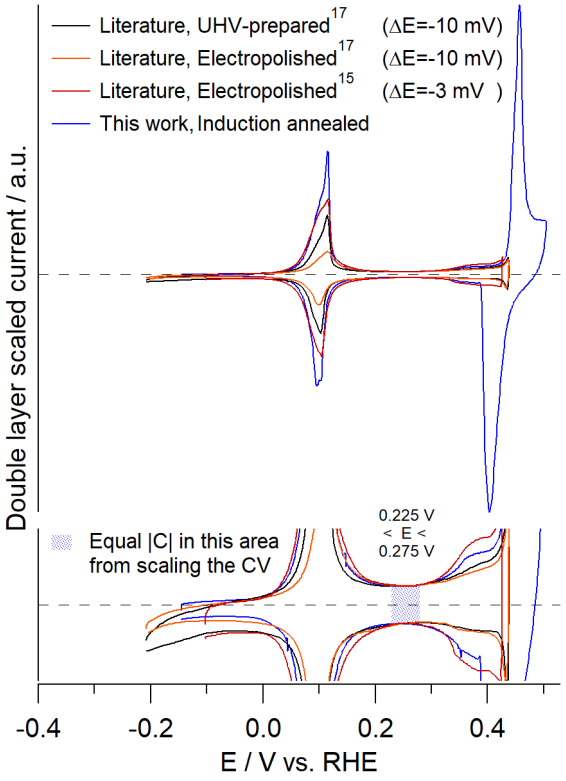

Figure 4.1: Comparison of literature reported CVs of Cu(111) with an induction annealing-prepared sample. CVs have been manually shifted up/down to reach the maximum amount of symmetry around the x-axis of the main adsorption features. CVs have been scaled to the absolute charge of the CV region represented by the blue dotted box, with the potential boundaries as specified in the image. δE values represent the amount by which literature CVs were manually adjusted to align the key adsorption feature at $+0.1!\ V$ with the induction annealed CV.

If this alternative measuring strategy would result in an increased number of terrace sites, and thereby yield increased charge of the adsorption feature (i.e., surface roughening), one would expect the double layer thickness (i.e., total surface capacitance) to similarly increase. However, normalizing by the charging current (as determined between $+0.225\ V < E < +0.275\ V$) does not resolve the charge discrepancy (e.g., compare the red and black lines). Considering this argument relies heavily on the assumption that certain regions of the CV are purely (pseudo-) capacitive in nature, we point to a publication by Maagaard *et al.*[13] wherein they show that introducing step-site defects in a Cu(111) crystal leads to (small) increases in the electro-sorption charge of the {111}-specific feature which is similarly reflected in a small increase in current in the double layer region we defined previously. Furthermore, their step-rich surface exhibits an additional oxidative feature near $+0.29\ V$ and cathodic feature near $-0.04\ V$, both of which

are not observed in our Cu(111) CV nor in those reported by Sebastián-Pascual *et al.*[15] Additional proof against electrochemical roughening comes from ref [18] where they show via ex-situ STM of a Cu(111) crystal pre- and post-electrochemical characterization ($0.1\ M$ KOH) that cycling between $-0.2\ V < E < +0.45\ V$ leads to *"…no major structural changes…, suggesting that the Cu(111) surface is relatively stable under these conditions"*.

An alternative explanation for the discrepancy in peak intensity might be that the CVs reported by Tiwari *et al.*[17] and Maagaard *et al.*[13] were measured in KOH electrolyte, whereas we and Sebastián-Pascual *et al.*[15] used NaOH electrolyte. However, those same authors (in the SI of another one of their publications[18]) report only minor differences for a CV of Cu(111) when measuring in either KOH or NaOH. Hence, also differences in the solution cations are unable to explain this difference. Therefore, we tentatively propose instead that the charge associated with this feature reflects the state of the surface in the electrochemical environment, with the increased intensity being an indicator of surface quality and long-range ordering of the atoms making up the terraces at the metal|electrolyte interface.

Further differences between UHV-prepared Cu(111) CVs and electropolished / induction annealed surfaces can be observed with regards to the amount of crystal defects (as visible from charge in the region $+0.32\ V < E < +0.42\ V$). To start, the orange (electropolished) CV actually exhibits a lower quantity of defect sites than the UHV-prepared surface by the same group (black). However, this surface also exhibits severe suppression of the main OH-adsorption feature, thus the defect density is still increased with respect to the UHV sample. The other non-UHV surfaces (red, blue) both exhibit increased amounts of defect sites as compared to the UHV-prepared surface, which is more in line with expectations considering that surface preparation involving electropolishing introduces defects into the surface. However, whereas generally defect density increases as a surface is electropolished more, the number of defect sites for our induction annealed surface was found to be stable with respect to time (not depicted) – even though periodic electropolishing was applied when an experiment resulted in irreversible surface changes. Actually, the majority of the defects present in the surface originated from our initial attempts at cleaning the crystal; a methodology which has since been replaced by a milder technique that introduces fewer defects.

Overall, a Cu(111) crystal prepared via induction annealing exhibits the features indicative of clean {111} terraces, with a relatively lower defect-to-terrace sites ratio ($Q_{defects} : Q_{terraces}$) than electropolished surfaces, although not as good as a UHV-prepared Cu(111) crystal. Furthermore, it was found (not depicted) that the quantity of step defects did not increase with additional electropolishing when post-induction annealing was employed, contrary to what is observed for surfaces that are not annealed after such treatment. Finally, it was observed that the exact electrochemical methodology has a strong influence on the intensity of the {111}-terrace specific OH-adsorption feature at ca. $+0.1\ V$, where shorter periods at a constant polarization potential followed by constant cycling result in more a pronounced feature. Similar sensitivity of Cu(111) with respect to the initial polarization period (potential and/or time) has been reported before[9], but in that work

the resulting CV exhibits clear signs of contamination associated with impurities related to alkaline glass leaching.[18] As such, it is unclear if the sensitivity towards the initial polarization time we observe in the absence of impurities is the result of the same phenomenon as the effect they observe in the presence of foreign surface adsorbates – especially considering that they also report the CV to evolve with successive cycling, which we do not observe.

Cu(100) literature comparison

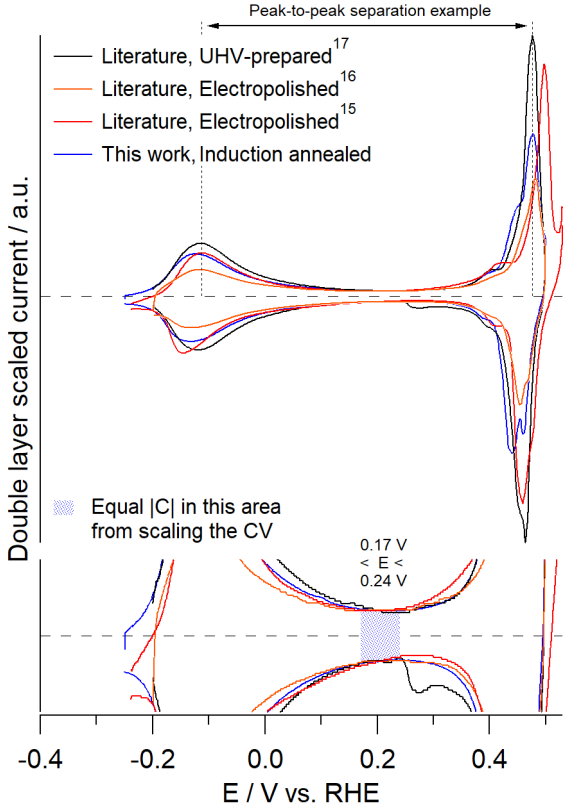

Figure 4.2: Comparison of literature reported CVs of Cu(100) with an induction annealing-prepared sample. CVs have been manually shifted up/down to reach the maximum amount of symmetry around the x-axis of the main adsorption features. CVs have been scaled to the absolute charge of the CV region represented by the blue dotted box, with the potential boundaries as specified in the image.

In Figure 4.2, CVs are depicted for Cu(100) as prepared via different methodologies. Black shows the electrochemical signal of a UHV-prepared surface[17], with an electropolished example by the same group in orange.[16] An electropolished surface published by Sebastián-Pascual *et al.* is shown in red[15], and finally the CV obtained by us via induction annealing is depicted in blue. The {100} facet exhibits two specific features: a reversible feature around $-0.1\ V$ ascribed to OH-

Table 4.1: Peak-to-peak separation of the two oxidative {100}-terrace adsorption features for the different Cu(100) crystals. These values are meant mostly for illustrative purposes, as they are of limited accuracy due to the transcription process converting images to numeric data.

Crystal	**Peak separation (mV)**	**Δ compared to UHV (mV)**
Cu(100), UHV (black)	591	0
Cu(100), Electropolished (orange)	597	6
Cu(100), Electropolished (red)	610	19
Cu(100), Induction annealed (blue)	599	8

adsorption[9, 17, 24, 25], and another reversible feature at ca. $+0.475\ V$[11] (which is likely due to O-adsorption, addressed in more detail in a later section). It is important to note that it has been reported that copper {100} terraces are not stable when cycled in the potential window used for electrochemical surface characterization[25] as commonly employed in prevalent literature and also in this work.[9–11, 17] However, it has recently been shown that adventitious oxygen in the electrolyte has a significant effect on the voltametric behavior of a Cu(100) surface[11], and large amounts of oxygen (as evidenced by the overall cathodic current) are observed in the work reporting about the instability of the terrace sites.[25] In this work, we shall presume that a Cu(100) surface is stable under the employed characterization conditions (as implied by the reproducibility of the CV with successive cycling, not depicted), so long as the electrolyte is properly deaerated.

The Cu(100) CVs from different sources show better agreement than in the case of Cu(111), exhibiting reasonably comparable intensities for the feature near $-0.1\ V$, although showing some more variability in the second feature (ca. $+0.475\ V$). Comparing the UHV-prepared surface (black) with the electropolished surface from the same group (orange) shows once again that the electropolished sample exhibits overall suppression of the facet-specific adsorption features. Additionally, it can be seen that the second feature is shifted to slightly more oxidative potentials (see also Table 4.1, where the peak-to-peak distance is given – with a visual representation of the meaning of this separation distance, using the UHV-sample as an example, given in Figure 4.2). Comparing the electropolished sample by Sebastián-Pascual *et al.*[15] (red) with the orange electropolished sample shows that the former exhibits more prominent OH-adsorption features, but at the cost of i) reduced symmetry of the feature near $-0.125\ V$, and ii) a more substantial shift of the second adsorption feature (Table 4.1).

If we compare the surface prepared via induction annealing (blue) with the other literature reported crystals, it is in-between the electropolished and UHV-prepared samples. E.g., the intensity of the feature at $-0.125\ V$ agrees well with that of the electropolished sample with more prominent features (red), but is suppressed in comparison to the UHV-prepared surface (black). But, the level of symmetry is greater than the red sample, matching that of the black sample. As for the second feature near $+0.475\ V$, we find that its location matches well with that of the UHV-prepared sample (though its peak-to-peak distance is still slightly increased,

Table 4.1), as opposed to the red trace which exhibits a significant shift towards more oxidative potentials. However, the intensity of the feature is lower than either of those surfaces – though it has been reported that this feature is very sensitive to the presence of trace amounts of oxygen in the solution, with higher peak intensities associated with increased oxygen content[11] (with our system having very little oxygen).

Comparing the same points with the second electropolished surface (orange) is more favorable, with the induction annealed surface better matching the features of a properly prepared UHV-sample in most instances though they both exhibit similar levels of symmetry for the first peak. Finally, it can be observed that the induction annealed CV has a shoulder near $+0.445\ V$ (its location matching well with the second feature of Cu(111)), which is more prominent than for the literature samples. Similar to Cu(111), we attribute this higher density of crystal defects in our sample to our initial crystal cleaning attempts and we expect these to be present to a lesser degree if new crystals are cleaned employing the alternative electropolishing procedure as described in the experimental section.

Overall, the CV of a Cu(100) crystal as-prepared via induction annealing is found to be a compromise between the CVs obtained after UHV surface preparation and electropolishing. The OH-adsorption feature near $-0.125\ V$ exhibits good symmetry, but is suppressed in intensity as compared to a UHV-prepared surface, though more pronounced and symmetrical than after electropolishing. The second {100}-terrace specific feature near $+0.475\ V$ is suppressed in intensity compared to all literature-reported surfaces (possibly related to differences in the amount of oxygen present in solution), but matches well in its location with that of a UHV-prepared surface. However, the amount of defect sites present in the crystal was significantly worse than the other surfaces – which we posit should not be as prominent if milder cleaning procedures are employed for newly procured crystals.

Cu(110) literature comparison

In Figure 4.3, various Cu(110) CVs are depicted with the signal of a UHV-prepared surface shown in black[17] and an electropolished crystal from the same group shown in orange,[16] an electropolished surface published by Huang *et al.* (likely measured in a glass cell) depicted in red[22], and the characterization CV obtained in this work via induction annealing shown in blue. This facet is reported to have two facet-specific regions; one OH-adsorption feature[17] located near $-0.3\ V$ and an additional feature near $+0.335\ V$ (for which we will discuss the corresponding adsorbates later). However, we found that scanning to the potential boundaries where the former peak is located resulted in severe suppression of the second feature. Increasing the lower potential boundary to more positive values resulted in more stable voltammetry at the cost of not seeing this cathodic feature at $-0.3\ V$. Considering the apparent instability of the CV in this wider potential window, combined with the fact that most published CVs stop at more positive potentials (including many of the Cu(110) CVs reported by the group that identified the feature at $-0.3\ V$[17]), we shall exclude this particular adsorption feature from our discussion.

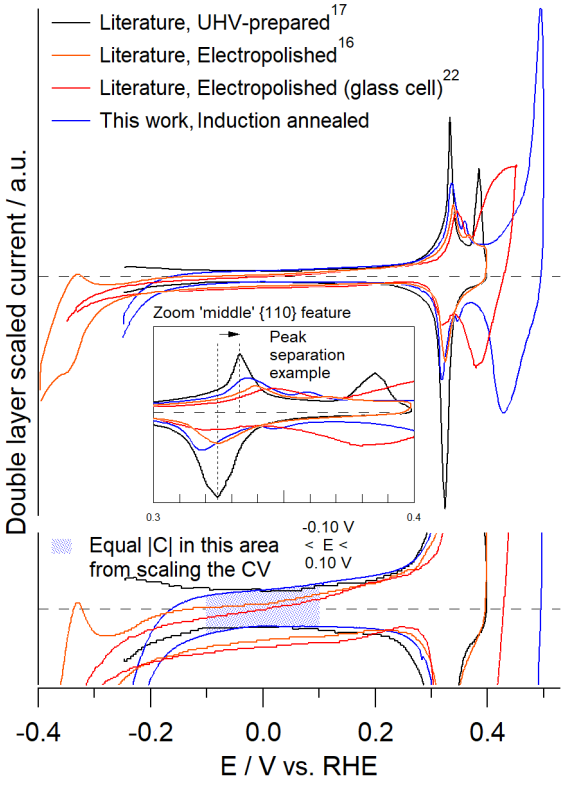

Figure 4.3: Comparison of literature reported CVs of Cu(110) with an induction annealing-prepared sample. CVs have been manually shifted up/down to reach the maximum amount of symmetry around the x-axis of the main adsorption features. CVs have been scaled to the absolute charge of the CV region represented by the blue dotted box, with the potential boundaries as specified in the image.

Starting with the electropolished crystal by Huang *et al.* (red)[22], we see a mostly featureless region between $-0.25\ V < E < +0.05\ V$ and a faint, broad feature between $+0.05\ V < E < +0.25\ V$ (the region where {111} terraces adsorb OH). Going more positive we find a symmetrical feature at ca. $+0.33\ V$ that is related to {110} terraces (a measure for the peak symmetry as visually represented in Figure 4.3, is given in Table 4.2). Finally, we observe a large oxidative 'hump' between $+0.35\ V < E < +0.45\ V$, which (to the best of our knowledge) is not specific to {110} terrace sites and we shall thus attribute to crystal defects. Next we shall discuss the electropolished sample reported by Tiwari *et al.*[16] (orange). Their CV exhibits a more symmetrical (Table 4.2) and comparatively sharper {110} feature, the same broad featureless region at lower potentials, and is missing most of the defect-related peaks present for the red crystal – although a scrutinizing eye can observe a faint reversible peak between $-0.25\ V < E < -0.05\ V$ (representing OH-adsorption on {100} terraces). However, the CV does have an additional feature in the form of a defect-related minor oxidative spike near $+0.367\ V$, although

Table 4.2: Peak separation between the maxima of the oxidative and reductive waves of the {110} feature at ca. $+0.33\ V$. These values are meant mostly for illustrative purposes, as they are of limited accuracy due to the transcription process converting images to numeric data.

Crystal	Peak separation (mV)
Cu(110), UHV (black)	9
Cu(110), Electropolished (orange)	15
Cu(110), Electropolished (red)	25
Cu(110), Induction annealed (blue)	18

no associated peak in the negative-going scan direction is observed (possibly it is irreversible to such an extent that it overlaps with the cathodic {110} feature).

A UHV-prepared crystal (black)[17] similarly shows a virtually featureless region between $-0.25\ V < E < +0.30\ V$, followed by a sharp, symmetrical {110}-related adsorption feature – although the cathodic wave exhibits increased charge compared to the anodic wave. At more positive potentials, an oxidative can be seen spike (ca. $+0.385\ V$) whose origin is not elaborated on in the original paper.[17] Seemingly, this spike has no counterpart in the negative-going scan direction, although it is likely potential-shifted due to non-reversibility and happens to overlap with the cathodic {110}-related feature, considering the charge mismatch between the cathodic and anodic waves of said feature. Interestingly, the location of the spike at $+0.385\ V$ matches well with where {100} step sites exhibit adsorption-related charge, as deduced from the reversible peak in this area present for the CV of a Cu(211) crystal.[16] However, that crystal does not exhibit the same shift (i.e. irreversibility) of the desorption wave to lower potentials. Possibly the UHV-prepared Cu(110) surface, under electrochemical conditions, exists in a (partially) reconstructed state that exposes {100} step-like surface sites, considering that ordinarily highly reversible adsorption features are observed for single crystalline surfaces (though this is speculative).

An induction annealed crystal (blue) is again a compromise; being somewhere in-between an electropolished and a UHV-prepared surface. The double layer region up to $+0.30\ V$ is mostly featureless, although a prominent reductive 'tail' (presumably HER) is observed at the lower end of the potential range, and a minor amount of {111} terraces can be argued to be present as judged from a small amount of excess charge in the potential region between $+0.05\ V < E < +0.25\ V$. A clear, reversible {110}-specific feature is observed, but its intensity is suppressed compared to the UHV-prepared sample, although more prominent than for the electropolished surfaces. A reversible defect-related spike is seen near $+0.36\ V$ (at slightly more cathodic potentials than what is observed for the orange sample, and symmetrical contrary to the orange CV). Furthermore, by extending the positive potential window, an additional (irreversible) {110}-terrace specific feature is observed at $+0.494\ V$. An interesting empirical finding is that the Cu(110) surface is relatively stable even when scanning to $+0.50\ V$, exhibiting reproducible voltammetry (not depicted).

A final consideration is with regards to the reversibility of the {110} feature,

with all non-UHV samples exhibiting decreased reversibility compared to a UHV-prepared surface (Table 4.2). However, considering the mismatch between the charge of the anodic and cathodic waves for the UHV sample, it is likely that the cathodic wave is a convolution of two features. This may influence the metric we use to represent peak symmetry (e.g., the potential difference between the maxima of the anodic and cathodic waves, respectively) depending on the exact location of the (hypothesized) secondary feature. Hence, we consider peak symmetry to be of limited value as a means of comparison.

4.3.2. Properties of induction annealed crystals

Cu(111)

We shall now briefly discuss the characteristic CV of an as-measured Cu(111) surface prepared by induction annealing, following the electrochemical methodology described in this work. To this end, a standalone CV of Cu(111) with different levels of magnification and varying degrees of x-axis compression is depicted in Figure 4.4. Firstly, it can be observed that there exist two apparent 'double layer' regions: places where seemingly only capacitive current is observed, namely between $-0.15\ V < E < 0\ V$ and between $+0.2\ V < E < +0.3\ V$. However, the charging current in these two windows is not identical and, considering that the second region exhibits larger currents, it is probable that this latter region is not purely capacitive in nature. Similar behavior is also visible in the literature, though in that work it is more evident at a scan rate of $100\ mV \cdot s^{-1}$.[13] We hypothesize that adsorption phenomena on {111} terrace sites with high step density take place in this region. This statement is based on two observations. Firstly, Maagaard *et al.* show that the CV for a Cu(111) surface develops an additional oxidative feature at ca. $+0.28\ V$ upon roughening of the surface.[13] Secondly, in a work discussing CO oxidation on Cu single crystals, Tiwari *et al.*[16] report an electropolished CV for Cu(211) (which has a 3x{111}{100} structure), which shows a very broad feature between ca. $-0.02\ V < E < +0.25\ V$ – a window that is basically an extension of the region where {111} terraces are normally observed. Hence, this region should preferably be avoided if one wishes to determine the double layer capacity (C_{DL}), with the lower potential window ($-0.15\ V < E < 0\ V$) being more suitable for that purpose.

A second observation is that it is entirely possible, in practice, to obtain oxygen-free CVs for this facet (and copper in general), although this does require a properly sealed cell and generous amounts of argon bubbling. The significance of this observation lies in the fact that most literature work has substantial amounts of oxygen present (as judged from a lack of symmetry around the x-axis, especially at lower potentials), and it is unclear what kind of influences the presence and/or reduction of oxygen may have on the stability and adsorption behavior of (different types of) copper (sites). Having ORR current contribute to the CV may also lead to a misinterpretation of copper-specific behavior. E.g., signs of early onset HER due to increasing the number of defect sites and/or the number of {110} terrace sites in a copper surface might be misinterpreted as reduction of trace amounts of oxygen (such behavior can be seen to occur in Figure 4.8).

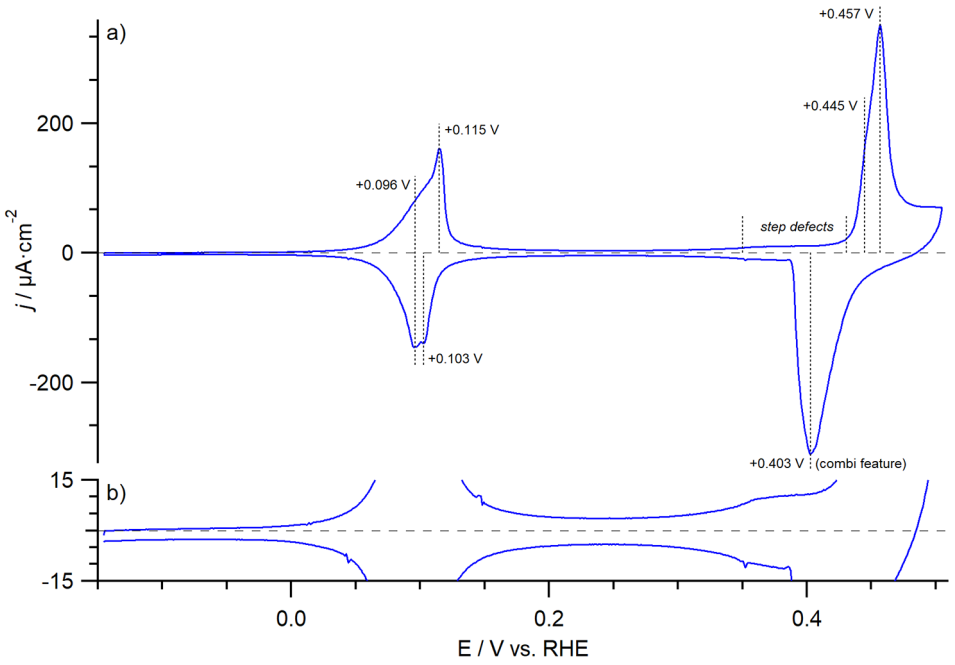

Figure 4.4: Normalized (geometric area) CV of Cu(111) as obtained after preparation via induction annealing, employing the electrochemical procedure described in the experimental section. Measured in $0.1\ M$ NaOH at scan rate $\nu = 50\ mV \cdot s^{-1}$.

As a third consideration, we shall discuss in more detail the {111} terrace-specific adsorption features in alkaline electrolyte. Specifically, there is the commonly reported[9, 10, 13, 17] reversible OH-sorption feature[12, 17, 23] near $+0.1\ V$ (peak A), which is actually a convolution of a broad peak located at more cathodic potentials and a narrower (i.e., sharper) peak located at more anodic potentials (ca. $+0.096\ V$ and $+0.115\ V$, respectively – Figure 4.4a). This binary nature is likely related to the average width of the terraces, as becomes evident when comparing the CV of a UHV-prepared surface (having large {111} terraces) with the CVs of electropolished Cu(111) (having overall smaller {111} terraces) (Figure 4.1, black vs. orange and red, respectively). From this, it can be seen that a UHV-prepared surface has a strong feature at $+0.115\ V$, and the broad peak at $+0.096\ V$ manifests as more of a shoulder, whereas electropolished surfaces are better described as consisting of mostly a broad feature, having a relatively smaller charge-contribution of the sharper spike at $+0.115\ V$.

Additionally, there exists a second, irreversible, adsorption feature at more oxidative potentials (ca. $+0.45\ V$, peak B) which is again best described as a convolution of two peaks: a peak centered around $+0.457\ V$, which has a shoulder at ca. $+0.445\ V$ (Figure 4.4a). Using similar reasoning, we ascribe this duality to O-adsorption on smaller and larger {111} terrace sites, where it is likely that the feature at $+0.445\ V$ is due to O-adsorption on smaller terraces as we observe

Table 4.3: Reaction schemes for OH and O adsorption on copper.

$$Cu_2O + H_2O + 2e^- \rightleftharpoons 2Cu + 2OH^-,\ E^0 = +0.41\ V \text{ vs. RHE } (pH13) \quad \text{(R1)}$$

$$nCu + OH^- \rightleftharpoons Cu_nOH_{ads} + e^- \quad \text{(R2)}$$

$$Cu_nOH_{ads} + OH^- \rightleftharpoons Cu_nO_{ads} + H_2O + e^- \quad \text{(R3)}$$

$$2CuOH \rightleftharpoons Cu_2O + H_2O \quad \text{(R4)}$$

this peak as well in the form of a defect peak in our Cu(100) crystal (Figure 4.5a). Considering the close proximity of this second feature to the equilibrium potential of Cu_2O formation ($+0.45\ V$ vs. $+0.41\ V$, Reaction R1 in Table 4.3[26]), it is likely that this feature is due to O-adsorption. If true, we would expect the charge associated with the OH-adsorption feature to be equal to the charge associated with the second feature as per the stoichiometry of Reactions R2 and R3 in Table 4.3 (where we have opted to not use "Cu_2O_{ads}" and "$CuOH_{ads}$" to avoid confusion with the formation of bulk oxides and CuOH, which is believed to be an existing but highly unstable species that is rapidly converted into Cu_2O via Reaction R4 in Table 4.3).[27–29] To substantiate the hypothesis that the second feature is related to O-adsorption, we mathematically deconvoluted the voltammogram into its individual constituents, which allows for an approximate quantification of the charges associated with each of the peaks that make up the CV (Figure C.8). From our deconvolution, we estimate that the ratio of peak A to peak B $\approx 0.9 : 1$, which we consider sufficiently close to the theoretically expected value of $1 : 1$ to tentatively assign this second adsorption feature to O-adsorption.

A final consideration is regarding the charge associated with the OH-adsorption feature. The value we calculate is equal to $107\ \mu C \cdot cm_{geo}^{-1}$, although this value does contain the charge contribution between $+0.1\ V < E < +0.25\ V$ as well (without this contribution, we find $101\ \mu C \cdot cm_{geo}^{-1}$). This value is significantly higher than the value reported by Tiwari *et al.*[17] ($79\ \mu C \cdot cm_{geo}^{-1}$) whose value corresponds to a coverage of 1/4th of a monolayer, with our calculated charge being closer to a coverage of 1/3rd of a monolayer instead. Considering that the OH-adsorption charge we find for the other basal planes agrees much better with literature (see next sections), and taking into account that this difference in charge for OH-adsorption on Cu(111) persists even when correcting for the double layer capacity (as discussed previously), we are currently unable to explain this discrepancy.

Cu(100)

The CV of an induction annealed Cu(100) surface as obtained in this work is given in Figure 4.5. Regarding the {100} specific features, a clear OH-adsorption feature[9, 17, 24, 25] is observed at ca. $-0.125\ V$ as is a (previously reported)[11] second feature near $+0.477\ V$. Regarding the nature of the adsorbing species for this anodic feature, we can use the same logic as previously. By mathematically deconvoluting the CV (Figure C.9), we find that the charge ratio of the OH-adsorption peak with

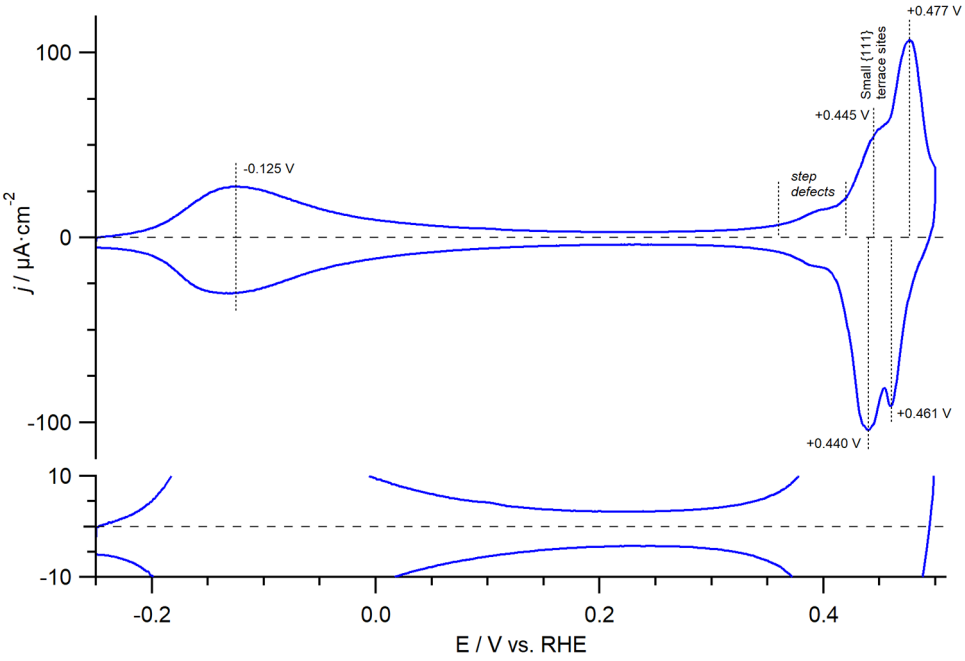

Figure 4.5: Normalized (geometric area) CV of Cu(100) as obtained after preparation via induction annealing, employing the electrochemical procedure described in the experimental section. Measured in $0.1\ M$ NaOH at scan rate $\nu = 50\ mV \cdot s^{-1}$.

respect to the second peak is (again) ca. $0.9 : 1$. Hence, we believe the feature at $+0.477\ V$ to be due to O-adsorption on {100}-terrace sites. Aside from this, we found (empirically) that the exact location of the second peak seems to depend on the quality of the surface (Figure 4.2), shifting to more oxidative potentials for surfaces with a higher defect density. As for the charge associated with the OH-adsorption feature, we find $68.7\ \mu C \cdot cm_{geo}^{-1}$ – which is in reasonable agreement with the theoretical value reported by Tiwari *et al.*[17] ($59\ \mu C \cdot cm_{geo}^{-1}$).

As a final consideration, we observe a larger-than-usual amount of defect sites in the form of a shoulder near $+0.445\ V$ (which we believe to be small {111} terrace sites), with literature reported CVs not commonly showing such an clear shoulder (though it is generally present, Figure 4.2). Interestingly, these terrace sites exhibit a much higher (apparent) reversibility than what we find for a Cu(111) crystal (Figure 4.4). Possibly, the reversibility of adsorption on these sites is a function of terrace size, with smaller terraces exhibiting increased reversibility. Alternatively, our assignment of this feature to {111} terraces might be erroneous, though we are not aware of any other surface sites that (may) give rise to an adsorption feature in this region. This peak was found to increase over time with repeated electropolishing under our initially employed electropolishing conditions (not depicted), but stabilized after switching to a milder electropolishing methodology (see experimental section). This milder form of electropolishing should result in better quality

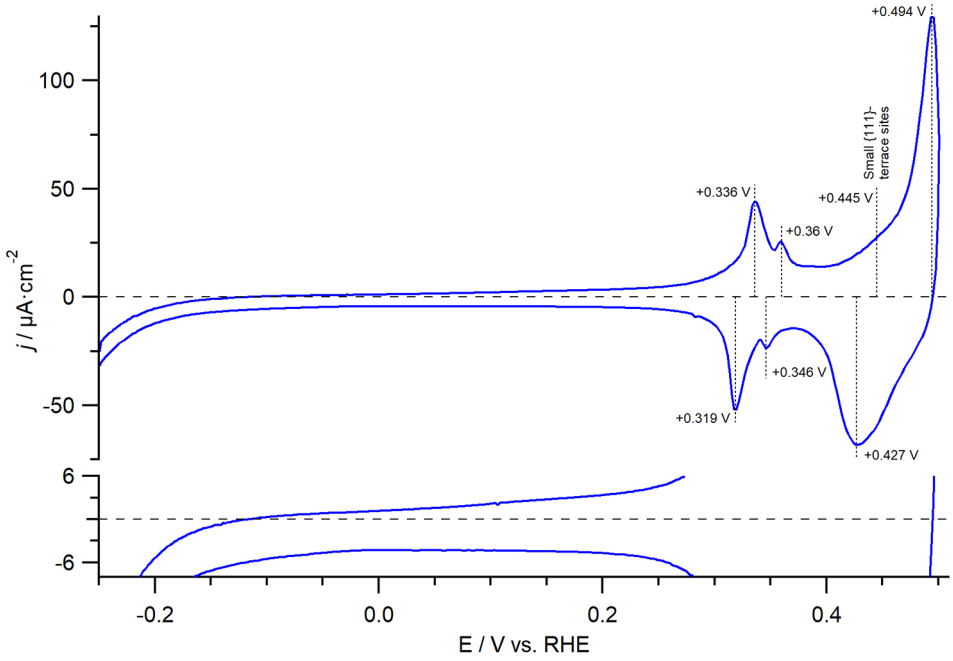

Figure 4.6: Normalized (geometric area) CV of Cu(110) as obtained after preparation via induction annealing, employing the electrochemical procedure described in the experimental section. Measured in $0.1\ M$ NaOH at scan rate $\nu = 50\ mV \cdot s^{-1}$.

surfaces with fewer defects.

Cu(110)

A typical characterization CV obtained for Cu(110) as obtained after induction annealing and electrochemical treatment as described in this work is depicted in Figure 4.6. Preparing this particular facet via induction annealing was found to be challenging, with strongly suppressed peak intensities observed for the {110}-specific feature after quenching the crystal in pure hydrogen (the default treatment employed for the other surfaces). Lowering the cooling rate, and/or changing the annealing atmosphere or cooling atmosphere all yielded similar results. Quench-cooling in pure argon looked promising, but resulted in the {110}-specific peak location shifting and becoming unstable during electrochemical cycling, transforming to yield the same suppressed CV as obtained in other instances. Eventually, we found that evolving large amounts of hydrogen (presumably) leads to restructuring of the surface to yield CVs with a peak intensity that compared favorably with literature. However, this methodology comes at a cost: preparing a Cu(110) crystal this way yields a CV that exhibits 'tailing' (likely HER) at potentials below $-0.1\ V$, which is not observed in published literature – although the presence of oxygen could potentially mask this effect to a certain extent.

Regarding the {110}-terrace specific peaks, a reversible adsorption feature is

observed at ca. $+0.33\ V$ and an additional irreversible feature is observed near $+0.494\ V$. Assigning the adsorbates associated with these two features is requires a bit more work than for the previous surfaces. OH-adsorption has been shown to correlate well with the potential of zero charge (pzc) for copper[15] with Cu(110) having the most negative pzc out of the three basal planes.[30] As such, the expected location of the OH-adsorption feature of Cu(110) would be at more negative potentials than for Cu(100) and Cu(111). To this end, Tiwari *et al.*[17] show that a {110}-specific adsorption feature exists at ca. $-0.3\ V$. However, the charge they determined experimentally to be associated with this feature is $25\ \mu C \cdot cm_{geo}^{-1}$, which is about half of the charge they expect based on their theoretical modeling ($54\ \mu C \cdot cm_{geo}^{-1}$). As their modelling predicts OH to bind atop the atoms making up the rows in the (110) surface, they conclude that Cu(110) likely exists in a (110)-(1x2) missing row reconstructed state, which would account for half of the charge missing. Interestingly, CV deconvolution (Figure C.10) of our system yields a very similar estimated charge for the feature at $+0.33\ V$ ($25.8\ \mu C \cdot cm_{geo}^{-1}$ vs. theoretically $27\ \mu C \cdot cm_{geo}^{-1}$). Furthermore, if we calculate the charge ratio of the peak with respect to the feature at $+0.494\ V$ (which we expect is related to O-adsorption), we find a ratio of ca. $1.06 : 2$. Finally, considering the equilibrium potential for Cu_2O formation ($+0.41\ V$, Reaction R1 in Table 4.3), it is rather unlikely that the feature at $+0.33\ V$ involves O-adsorption. Rather, it is more probable to be related to OH-adsorption.

Combining all these considerations can reasonably be done in two possible ways. Firstly, it is possible that a second, {110} terrace-specific, OH-adsorption site exists for a Cu(110)-(1x2) surface – which would likely be the surface sites that are exposed after removing every other row of atoms. In this case, a difference in adsorption strength would result in differing peak locations, but a similar total charge may be observed if the adsorbates are spaced approximately equally as in the case for adsorption on the top of the row. An alternative possibility is a potential-induced lifting of the reconstruction, where the surface reverts back to a Cu(110) surface at more anodic potentials. In such a case, an adsorption feature would be expected after lifting of the reconstruction, equal in charge to the first feature. Both instances would result a ratio of $1 : 2$ when calculating the ratio between either of the two cathodic (OH-adsorption) features and the adsorption feature at $+0.494\ V$, if the latter is O-adsorption. Although we cannot determine which of these options is correct from the current data, based on these evidences we are fairly confident in assigning the feature at $+0.33\ V$ to OH-adsorption and the feature at $+0.494\ V$ to O-adsorption.

4.3.3. Cu(poly): induction annealing vs electropolishing

Depending on research objectives it may be important to study surfaces that encompass all types of sites simultaneously, for instance as a means of determining the overall catalytic properties of a material in one measurement. Polycrystalline surfaces lie at the heart of such experiments as they consist of, by definition, many different crystallites of various orientations and dimensions. Though polycrystalline surfaces are more often than not studied for their relative simplicity, a properly conducted study using such surfaces can still provide a wealth of information on the overall behavior of a given material.

The methodology for preparing such polycrystalline copper surfaces generally encompasses procuring a sheet of material, machining it to the desired shape and dimensions, and then mechanically polishing it as a means of both decreasing the roughness factor (R_f = EASA/geometric area) as well as cleaning of the surface. An electrode prepared as such is expected to yield reasonably reproducible surfaces, so long as the starting material is of comparable purity. However, it is known that mechanically polished copper surfaces (even after sonication) do not yield CVs exhibiting the expected adsorption features of a copper surface,[11, 31] which can be interpreted as the copper surface being blocked by residues of the polishing process. Hence, an additional (anisotropic) electropolishing step is often applied, wherein the copper surface is oxidized in concentrated (phosphoric[2, 10]) acid solution and the electrogenerated oxides subsequently dissolve.[20] However, because the exact surface treatments employed by different laboratories vary slightly (e.g., polishing with finer slurries or different polishing materials, sonicating for varying time periods possibly in different solvents, electropolishing at different potentials or in electrolytes of differing compositions), reported characterization CVs for copper exhibit large differences between different laboratories, yet are all called polycrystalline.[11] In this work, we found that preparing polycrystalline spherical bead-type copper electrodes via induction annealing is an easy and quick method for producing clean copper surfaces with a consistent and wide site distribution that exhibit single-crystal like adsorption features when following the surface preparation and electrochemical procedure described in the experimental section.

In Figures 4.7a and 4.7b, we present the CVs of a mechanically polished + electropolished copper disk electrode ($Cu(poly)_{Mech}$) and an induction-grown + induction annealed spherical bead electrode ($Cu(poly)_{Induct}$) in red and blue, respectively. Both were measured as per the electrochemical methodology described in the experimental section. To verify that the differing normalization techniques between these two samples (geometric vs. electrochemically active area, see experimental section) would not influence the result we determined the roughness factor of the disk-type electrode from its OH-adsorption charge, finding $R_f = 1.02$ – which we believe is sufficiently close for fair comparison. The $Cu(poly)_{Mech}$ CV does exhibit some residual oxygen for which we are unsure to what degree it affects the differences we shall discuss. We shall proceed assuming it is of negligible influence.

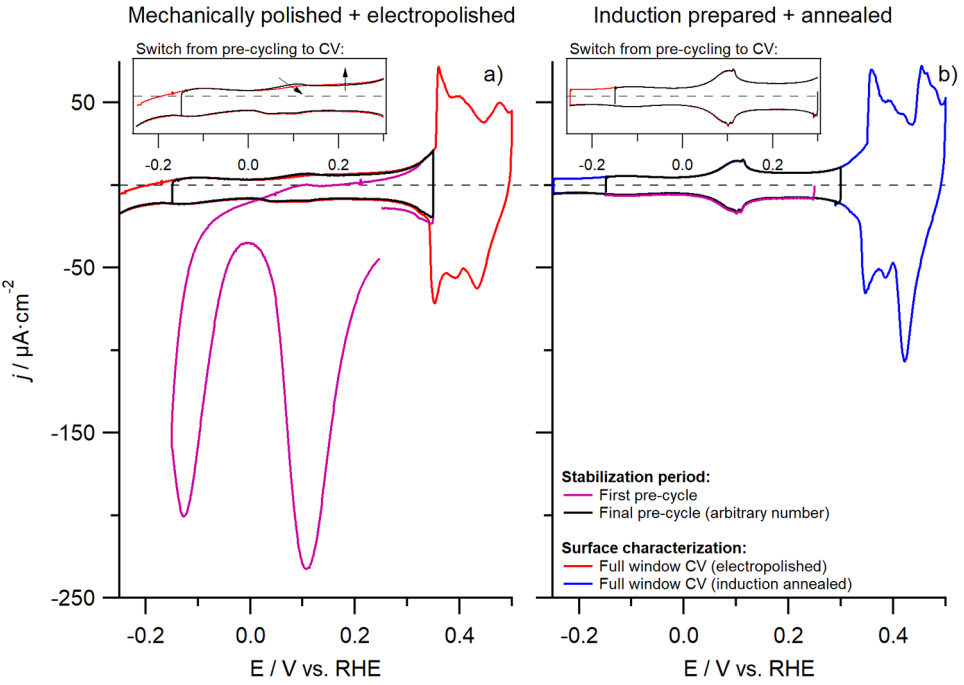

Figure 4.7: Typical copper CV ($0.1\ M$ NaOH, scan rate $\nu = 50\ mV \cdot s^{-1}$) obtained after a) mechanical polishing + electropolishing treatment and b) induction annealing treatment. In purple, the first CV after establishing electrolyte contact is depicted, while the last pre-characterization cycle (i.e., initial cycling in a smaller potential window to stabilize the surface and remove oxygen) is depicted in black. In red and blue are shown the full-window characterization CVs for the electropolished and induction annealing-prepared surfaces, respectively.

The greatest difference between these two samples can be seen in the first pre-cycling CV (purple); namely, that an electropolished electrode is initially covered by a layer of copper oxide, whereas the induction annealed surface is not. Though the former can be considered unavoidable under normal laboratory conditions (having to expose the electrode to ambient conditions for brief periods), it affects the surface. Specifically, the {111} terrace OH-adsorption feature at $+0.1\ V$ significantly differs between the red and blue CVs, both in shape and in intensity. Whereas this feature is reminiscent of a Cu(111) single crystal (Figure 4.1) for the $Cu(poly)_{Induct}$ electrode, the $Cu(poly)_{Mech}$ disk is found to exhibit less overall charge in this area, irreversibility, and a cathodic feature that seems split into two. This split is also observed if 'long' (ca. $> 10\ s$) standby potentials ($E = -0.25\ V$) are applied to surfaces containing {111} terrace sites (including Cu(111)) (Figure C.2), though the $Cu(poly)_{Mech}$ electrode was not subjected to such treatment. Hence, it is likely that the peak splitting is instead related to i) the electropolishing step or ii) the initial presence of an oxide film. Additional changes related to this peak arise when the lower vertex potential is decreased from $-0.15\ V$ to $-0.25\ V$ (compare the low potential region of the red and blue lines). In the case of a $Cu(poly)_{Induct}$

surface, we find that decreasing the lower potential boundary has negligible effect on the CV, whereas in the case of a Cu(poly)$_{Mech}$ surface we find that it leads to a redistribution of the charge of the anodic at ca. $+0.1\ V$ feature to overall more cathodic potentials (illustrated by the arrows in the inset in Figure 4.7a).

Overall, it can be said that the {111} terrace sites present on the surface of an electropolished electrode do not exhibit behavior that is representative of well-ordered, large {111} terraces; even though it is clearly possible to obtain an electrochemical signal reminiscent of the behavior of well-defined terraces with a polycrystalline electrode as evidenced by the CV for an induction annealed surface. Considering that the OH-adsorption behavior of {111} terrace sites on an electropolished surface differs from that observed for a Cu(111) crystal, it is likely that their electrochemical properties (e.g., catalytic activity) similarly differ to a certain extent.

The second important difference between the two polycrystalline surfaces is their facet distribution, as evidenced by the various peaks in the CV, and the relative charges associated with those peaks (with respect to one another). Specifically, besides OH-adsorption on {100} and {111} terrace sites ($-0.125\ V$ and $+0.1\ V$, respectively), a copper surface also exhibits a number of (distinct) peaks between $+0.35\ V < E < +0.50\ V$, whose individual current densities differ significantly between the two electrodes. That particular potential window can be split into two regions. Firstly, there is the window between $+0.35\ V < E < +0.44\ V$, which can be assigned to (OH-)adsorption on various step sites by realizing that this window is where single crystals of the principal orientations show charge unrelated to their primary sites (i.e., defect sites). Likely the adsorbate is OH, as the CV up to $+0.44\ V$ is found to be reversible (see e.g., Figures C.3 and C.7) and the alternative (O-adsorption) is generally irreversible (previously discussed) – though it can theoretically be either when taking into consideration the potential. The second region is between $+0.44\ V < E < +0.50\ V$ and is the region where O-adsorption on the terraces is observed.

Both regions exhibit clear differences when comparing the two surfaces, which can be interpreted as these surfaces having differing (ratios of) electrochemically active sites. These differences in surface facet distribution can likely be attributed to the anisotropic nature of the electropolishing step, where such treatment results in surfaces having a changed (preferential) site distribution compared to the starting surface. Considering that anisotropy favors certain types of sites over other types of sites, it involves both the preferential creation as well as the preferential removal of particular sites, where specifically the removal of sites may invalidate the measurement if e.g., the purpose of the experiment is to obtain the average activity of all possible sites simultaneously. The methodology for preparing a bead-type electrode which does not have such bias in surface site distribution is described in the SI.

Finally, induction annealing of a polycrystalline surface enjoys the same advantage as induction annealing copper single crystals; namely high surface reproducibility. A polycrystalline surface is the best way of illustrating reproducibility, exactly because it contains a wide assortment of different types of surface sites.

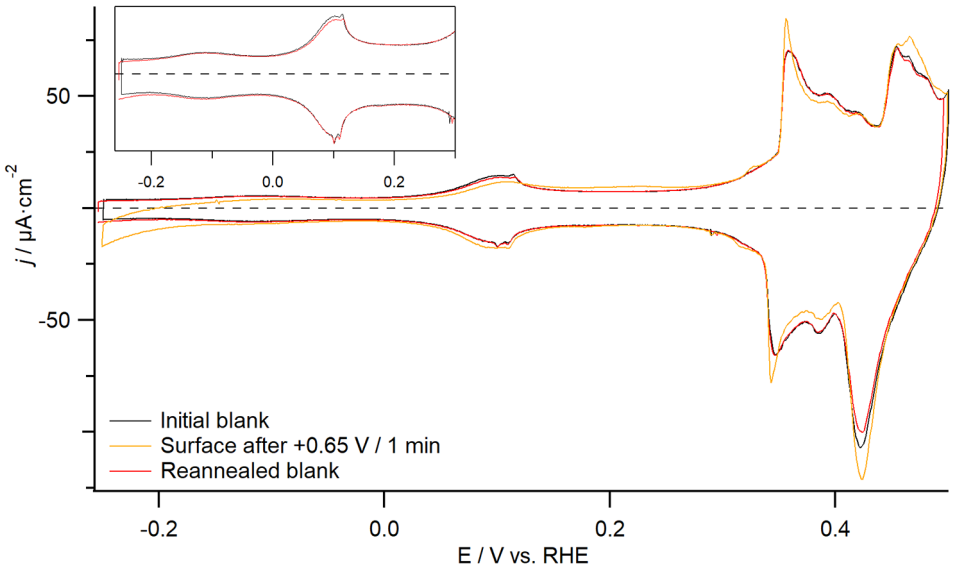

Figure 4.8: Illustration of the reproducibility of a polycrystalline surface after having been regenerated via induction annealing-treatment. In black, the initially obtained CV is depicted, whereas in orange the state of the surface is depicted after having been oxidized at $+0.65\ V$ for $60\ seconds$ in $10\ M$ NaOH. In red, the surface has been reannealed to recover its initial state. All CVs were measured in $0.1\ M$ NaOH at scan rate $\nu = 50\ mV \cdot s^{-1}$.

This is illustrated in Figure 4.8, where we depict the CV of an induction annealed Cu(poly) CV as obtained initially (black), after having been oxidized at $+0.65\ V$ for $60\ seconds$ in $10\ M$ NaOH (orange), and after having been reannealed and characterized again (red). The oxidative treatment introduces a clear change in the facet distribution at the interface (compare black to orange). However, after reannealing, the surface is fully recovered to its initial state (compare red and black) seeing as these CVs are virtually indistinguishable from one another (with the difference in the negative going scan being due to a slight mismatch in the anodic potential).

4.4. Conclusions

In this work, we cleaned and prepared copper single crystalline surfaces via a combination of electropolishing, induction annealing and very detailed electrochemical surface characterization methods. These methodologies were found to yield reproducible CVs, where the number of crystal defects did not increase with time. Furthermore, the CVs obtained in this manner compared favorably with literature reported CVs, although the quality was generally not on par with UHV-prepared surfaces. However, they were found to be of higher quality than what is reported for electropolished surfaces.

Induction annealing was also applied to polycrystalline surfaces, and a decreased site bias was observed compared to electropolished samples. Furthermore,

induction annealing was found to be capable of recovering even significantly altered surfaces such as after anisotropic oxidation/reduction cycles.

References

[1] Yoshio Hori, Katsuhei Kikuchi, and Shin Suzuki. Production of CO and CH4 in electrochemical reduction of CO2 at metal electrodes in aqueous hydrogencarbonate solution. *Chemistry Letters*, (11):1695–1698, 1985.

[2] Kendra P. Kuhl, Etosha R. Cave, David N. Abram, and Thomas F. Jaramillo. New insights into the electrochemical reduction of carbon dioxide on metallic copper surfaces. *Energy & Environmental Science*, 5(5):7050–7059, 2012.

[3] Hori Yoshio, Kikuchi Katsuhei, Murata Akira, and Suzuki Shin. Production of methane and ethylene in electrochemical reduction of carbon dioxide at copper electrode in aqueous hydrogencarbonate solution. *Chemistry Letters*, 15(6):897–898, 1986.

[4] Y. Hori, I. Takahashi, O. Koga, and N. Hoshi. Electrochemical reduction of carbon dioxide at various series of copper single crystal electrodes. *Journal of Molecular Catalysis A: Chemical*, 199(1):39–47, 2003.

[5] Ichiro Takahashi, Osamu Koga, Nagahiro Hoshi, and Yoshio Hori. Electrochemical reduction of CO2 at copper single crystal Cu(S)-[n(111)×(111)] and Cu(S)-[n(110)×(100)] electrodes. *Journal of Electroanalytical Chemistry*, 533(1–2):135–143, 2002.

[6] Federico Calle-Vallejo and Marc T. M. Koper. Theoretical considerations on the electroreduction of CO to C2 species on Cu(100) electrodes. *Angewandte Chemie International Edition*, 52(28):7282–7285, 2013.

[7] F. Sloan Roberts, Kendra P. Kuhl, and Anders Nilsson. High selectivity for ethylene from carbon dioxide reduction over copper nanocube electrocatalysts. *Angewandte Chemie*, 127(17):5268–5271, 2015.

[8] V. D. Jović and B. M. Jović. EIS and differential capacitance measurements onto single crystal faces in different solutions: Part II: Cu(111) and Cu(100) in 0.1 M NaOH. *Journal of Electroanalytical Chemistry*, 541:13–21, 2003.

[9] Vladimir Jović and Borka Jović. Surface reconstruction during the adsorption/desorption of oh species onto Cu(111) and Cu(100) in 0.1 M NaOH solution. *Journal of the Serbian Chemical Society*, 67(7):531–546, 2002.

[10] Klaas Jan P. Schouten, Elena Pérez Gallent, and Marc T.M. Koper. The electrochemical characterization of copper single-crystal electrodes in alkaline media. *Journal of Electroanalytical Chemistry*, 699:6–9, 2013.

[11] Albert K. Engstfeld, Thomas Maagaard, Sebastian Horch, Ib Chorkendorff, and Ifan E. L. Stephens. Polycrystalline and single-crystal Cu electrodes: Influence

of experimental conditions on the electrochemical properties in alkaline media. *Chemistry – A European Journal*, 24(67):17743–17755, 2018.

[12] Alexander Bagger, Rosa M. Arán-Ais, Joakim Halldin Stenlid, Egon Campos dos Santos, Logi Arnarson, Kim Degn Jensen, María Escudero-Escribano, Beatriz Roldan Cuenya, and Jan Rossmeisl. Ab initio cyclic voltammetry on Cu(111), Cu(100) and Cu(110) in acidic, neutral and alkaline solutions. *ChemPhysChem*, 20(22):3096–3105, 2019.

[13] Thomas Maagaard, Aarti Tiwari, Ib Chorkendorff, and Sebastian Horch. On the possibilities and considerations of interfacing ultra-high vacuum equipment with an electrochemical setup. *ChemPhysChem*, 20(22):3024–3029, 2019.

[14] Paula Sebastián-Pascual, Stefano Mezzavilla, Ifan E. L. Stephens, and María Escudero-Escribano. Structure-sensitivity and electrolyte effects in CO2 electroreduction: From model studies to applications. *ChemCatChem*, 11(16):3626–3645, 2019.

[15] Paula Sebastián-Pascual, Francisco J. Sarabia, Víctor Climent, Juan M. Feliu, and María Escudero-Escribano. Elucidating the structure of the Cu-alkaline electrochemical interface with the laser-induced temperature jump method. *The Journal of Physical Chemistry C*, 2020.

[16] Aarti Tiwari, Hendrik H. Heenen, Anton Simon Bjørnlund, Degenhart Hochfilzer, Karen Chan, and Sebastian Horch. Electrochemical oxidation of CO on Cu single crystals under alkaline conditions. *ACS Energy Letters*, 5(11):3437–3442, 2020.

[17] Aarti Tiwari, Hendrik H. Heenen, Anton Simon Bjørnlund, Thomas Maagaard, EunAe Cho, Ib Chorkendorff, Henrik H. Kristoffersen, Karen Chan, and Sebastian Horch. Fingerprint voltammograms of copper single crystals under alkaline conditions: A fundamental mechanistic analysis. *Journal of Physical Chemistry Letters*, 11(4):1450–1455, 2020.

[18] Aarti Tiwari, Thomas Maagaard, Ib Chorkendorff, and Sebastian Horch. Effect of dissolved glassware on the structure-sensitive part of the Cu(111) voltammogram in KOH. *ACS Energy Letters*, 4(7):1645–1649, 2019.

[19] J. Clavilier, R. Faure, G. Guinet, and R. Durand. Preparation of monocrystalline Pt microelectrodes and electrochemical study of the plane surfaces cut in the direction of the {111} and {110} planes. *Journal of Electroanalytical Chemistry and Interfacial Electrochemistry*, 107(1):205–209, 1980.

[20] G. Yang, B. Wang, K. Tawfiq, H. Wei, S. Zhou, and G. Chen. Electropolishing of surfaces: theory and applications. *Surface Engineering*, 33(2):149–166, 2017.

[21] Alexander Bagger, Logi Arnarson, Martin H. Hansen, Eckhard Spohr, and Jan Rossmeisl. Electrochemical CO reduction: A property of the electrochemical interface. *Journal of the American Chemical Society*, 141(4):1506–1514, 2019.

[22] Yun Huang, Albertus D. Handoko, Pussana Hirunsit, and Boon Siang Yeo. Electrochemical reduction of CO2 using copper single-crystal surfaces: Effects of CO* coverage on the selective formation of ethylene. *ACS Catalysis*, 7(3):1749–1756, 2017.

[23] V. Maurice, H. H. Strehblow, and P. Marcus. In situ STM study of the initial stages of oxidation of Cu(111) in aqueous solution. *Surface Science*, 458(1):185–194, 2000.

[24] B. J. Cruickshank, Douglas D. Sneddon, and Andrew A. Gewirth. In situ observations of oxygen adsorption on a Cu(100) substrate using atomic force microscopy. *Surface Science*, 281(1):L308–L314, 1993.

[25] Julia Kunze, Vincent Maurice, Lorena H. Klein, Hans-Henning Strehblow, and Philippe Marcus. In situ STM study of the anodic oxidation of Cu(001) in 0.1 M NaOH. *Journal of Electroanalytical Chemistry*, 554-555:113–125, 2003.

[26] William M. Haynes, David R. Lide, and Thomas J. Bruno. *CRC handbook of chemistry and physics: a ready-reference book of chemical and physical data*. 97 edition, 2017.

[27] S. M. Abd el Haleem and Badr G. Ateya. Cyclic voltammetry of copper in sodium hydroxide solutions. *Journal of Electroanalytical Chemistry and Interfacial Electrochemistry*, 117(2):309–319, 1981.

[28] Marcel Pourbaix. Atlas of electrochemical equilibria in aqueous solution. *NACE*, 307, 1974.

[29] Inna L. Soroka, Andrey Shchukarev, Mats Jonsson, Nadezda V. Tarakina, and Pavel A. Korzhavyi. Cuprous hydroxide in a solid form: does it exist? *Dalton Transactions*, 42(26):9585–9594, 2013.

[30] O. Koga, T. Matsuo, N. Hoshi, and Y. Hori. Charge displacement adsorption of carbon monoxide on [110] zone copper single crystal electrodes in relation with PZC. *Electrochimica Acta*, 44(6):903–907, 1998.

[31] David Reyter, Marek Odziemkowski, Daniel Bélanger, and Lionel Roué. Electrochemically activated copper electrodes: surface characterization, electrochemical behavior, and properties for the electroreduction of nitrate. *Journal of the Electrochemical Society*, 154(8):K36, 2007.